Hindawi
Geofluids
Volume 2021, Article ID 8813743, 15 pages
https://doi.org/10.1155/2021/8813743

Research Article

Experimental Study of Joint Roughness Influence on Fractured Rock Mass Seepage

Zhongxi Tian,[1] **Chunquan Dai**,[2] **Qingshuang Zhao**,[1] **Zhaobo Meng**,[1] **and Baoliang Zhang**[1]

[1]*College of Architecture and Civil Engineering, Liaocheng University, Liaocheng 252000, China*
[2]*College of Civil Engineering and Architecture, Shandong University of Science and Technology, Qingdao 266590, China*

Correspondence should be addressed to Zhongxi Tian; 391838343@qq.com

Received 11 August 2020; Revised 23 September 2020; Accepted 9 February 2021; Published 28 February 2021

Academic Editor: Andrew H. Manning

Surrounding rock pressure, water pressure, and joint roughness are the important factors that affect the fractured rock mass seepage. It is of great significance to quantify the influence of these factors through experiments. In this study, rock fracture joint surfaces were measured. Next, 3D coordinates of joint surfaces were extracted with using the Geomagic software, and joint roughness was described using the mean variance of protrusion height and equidistant fluctuation angle, which were acquired through calculation. Stress-seepage coupling test was then conducted on the samples on a triaxial apparatus, and the effects of confining stress and water pressure on the permeability of single-fracture rock were investigated. On the basis of the relationship between the parameters in data fitting expression and the mean variance of protrusion height and equidistant fluctuation angle, the calculation formula of the permeability coefficient including joint roughness, confining pressure, and seepage pressure difference was derived.

1. Introduction

Rock mass is a complex natural geological body composed of intact rock and jointed spaces at various scales. After underground rock mass is excavated, surrounding rock is disturbed, and the joints increase. The change in the stress distribution of surrounding rock has an effect on fractured rock mass seepage. The seepage affects the stress distribution in surrounding rock, and the stress and seepage fields in surrounding rock produce a coupling effect. Their coupling significantly affects the permeability characteristics of rock mass and engineering stability. Therefore, studying the coupling effect between stress and seepage fields during seepage is important.

The study of coupling between stress and seepage fields in fractured rock mass is based on single-fracture rock mass. Snow and Louis [1–3] researched on the seepage law of single fracture and proposed the cubic law and a series of correction methods based on Navier–Stokes equation. Wang et al. [4] used the employment of the fractal dimension of joint surface to improve equation involving the relation between mechanical aperture and hydraulic aperture and carried out experimental verification. Vogler et al. [5] investigated the effect of fracture heterogeneity on fluid flow through fractures and captured the relationship between fracture closure behavior and fluid pressure. Zhao et al. [6] used digital image technology to extract the spatial distribution information of fractured rock mass. They established 3D digital analysis models to obtain interconnected networks of spatial structures and spatial distribution characteristics of stress, seepage, and speed. The approximate calculation and experimental study showed that particle size has a great influence on fractured rock mass seepage.

Wang et al. [7, 8] experimentally investigated nonlinear flow characteristics of rough-walled fractures during shear process under different boundary conditions and analyzed the effects of shear process, fracture surface roughness, boundary normal stiffness, and initial normal stress on nonlinear flow behaviors. Tatone and Grasselli [9] performed

digital analysis of fracture surface in situ and found that fracture roughness increased with the sampling window size. Zou et al. [10] developed wavelet analysis technique to solve Navier–Stokes equation without linearization and decomposed the original wall surface roughness profiles of a fracture into high- and low-frequency profiles. The results indicated that in addition to the Reynolds number, the high-frequency secondary roughness is the main cause for the dynamic evolution of eddy flow regions in the fracture flow field. Jiang et al. [11] proposed the empirical formula for the relationship between mechanical and hydraulic openings of fracture joints; however, no sufficient evidence exists that the formula quantitatively describes the effectiveness of stress seepage coupling. Wang et al. [12] used the particle flow code (PFC) to simulate the shear test of rock joint with different joint roughness, under constant normal load (CNL) and constant normal stiffness (CNS) boundary conditions, in order to assess the macro- and mesomechanical properties and failure mechanism of rock joints subjected to shear. Zhang et al. [13] developed the testing system displaying the development process of floor fractures and the formation of water inrush channels and proposed that the floor was in a state of high shear stress under the action of rock stress and high pressure confined water, which was likely to cause shear fracturing and consequently possible water inrush into the mine working faces.

The relationship between permeability and confining or axial pressure can be presented using a three-axis apparatus. This apparatus is used to perform seepage test on single-fracture rock samples subjected to axial compression fracturing. Lyu et al. [14] developed a seepage module of rock triaxial servo tester to realize the rock seepage test under 3D stress condition. Liu et al. [15] used an ELE rock osmometer for axial compression crack, artificial smooth fracture, and artificial smooth filling fracture. They conducted seepage tests under different confining and axial pressures and compared and analyzed the difference of the three seepage characteristics. However, they did not consider the rough filling fracture.

Yu et al. [16] studied the seepage characteristics of single-fracture sandstone with axial compression cracking under loading and unloading conditions. The results showed that the effective confining pressure decreases, whereas the seepage permeability rises but is less than the original path. The relationship between permeability and effective confining pressure was embedded into the finite element model; however, joint roughness was not considered in the numerical simulation. Porous sandstone with fracture was regarded as double-porous media. Souley et al. [17] adapted an experimental device to measure flow through porous rock mass samples in addition to fracture flows. They used VIPLEF/-HYDREF numerical codes considering the dual-porosity of the sample (fracture and rock matrix) to reproduce hydromechanical loading.

Describing the fracture joint roughness quantitatively in axial compression can be difficult. The rough fracture formed by Brazilian splitting can be considered approximately as the rock tensile fracture in nature [18, 19], which is beneficial to the measurement of joint roughness. This method also provides an ideal fracture form for single-fracture seepage test. Liu et al. [20] performed a seepage test of split sandstone through an ELE rock permeation instrument. Their results indicated that under the stress path of constant confining pressure and gradual water pressure loading, permeability coefficient and water pressure have a linear growth relationship, whereas permeability coefficient and confining pressure have a negative exponential relationship. Han [21] obtained similar test results through a large number of seepage tests of single and vertical intersecting fracture rock masses. However, they did not further establish the functional relationship between permeability coefficient and joint roughness. Tian et al. [22] derived the theoretical calculation formula of the permeability coefficient when different lithology rocks were located on two sides of single-fracture rock and validated the formula by simplifying the forces applied in the test.

Controlling the seepage test process is difficult, and its success rate is low due to a lack of clear criteria for success. In the present study, the Brazilian splitting test method was improved through in situ sampling. A seepage test for a single fracture was performed using a TAW-2000M rock triaxial servo instrument. The effects of confining pressure, water pressure, and joint roughness on the seepage law of rough fracture were studied, and the seepage mechanism was explored.

2. Sample Preparation and Measurement of Joint Roughness

2.1. Sample Preparation. Coarse sandstone (CS), fine sandstone (FS), and mudstone (MS) were initially processed into standard cylindrical rock samples ($\Phi 50 \times 100$ mm). These samples were obtained from the Fucheng Coal Mine in Inner Mongolia. Samples with similar texture, no impurity, no damage, no crack, and their integrity were screened using a magnifying glass, and these samples were weighed. On the basis of lithology, the samples were divided into CS, FS, and MS, each group comprising of six samples. The modified Brazilian splitting jig was used to split the samples on the TAW-2000M rock triaxial servo instrument, and the cylindrical samples with through single fracture were obtained. The splitting steps of the sample are described as follows.

First, a certain preload was applied to the sample according to a loading manner, and the preloading value was 1 kN

Second, the fixed splints were loosened on both sides after preloading, and the sample was fixed by the upper and lower blades

Third, the axial pressure was applied in a displacement approach. The speed of the blade cleavages was 0.05 mm/min, and the target was 5 mm. After splitting the samples, tensile crack was formed, as shown in Figure 1

After splitting, second weighing and screening were performed, and the samples with large mass loss and breakage were removed. When each group of the samples was less than 6, it must be supplemented.

Due to the different lithology, the joint roughness of samples after splitting is relatively different. The CS sample has a large particle size, a rough surface, and minimal overall surface fluctuation. The FS has a small particle size, a smoot

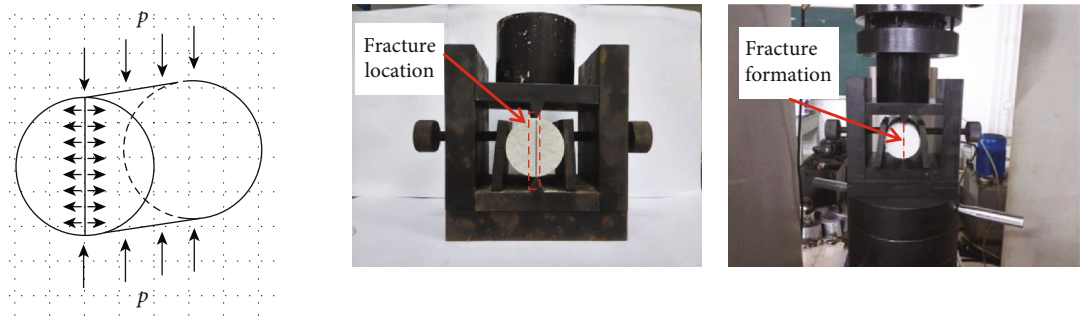

(a) Schematic of Brazilian splitting method (b) Modified Brazilian splitting jig (c) Sample splitting

Figure 1: Loading device and loading diagram of modified Brazil splitting.

surface, and is greatly overall surface undulating. The MS has a fine particle size and a sharp surface, with many twists and steeps. These characteristics are shown in Figure 2.

2.2. Measurement of Joint Roughness. Joint roughness has important influence on the seepage of fractured rock mass, and its measuring method has always been an important aspect for fracture seepage research. The height and slope of the joint surface are objective indicators for describing joint roughness. The slope is generally described by the fluctuation angle. In this study, the datum plane was set up, longitudinal and transverse equidistant spline lines were adopted, and the variance of protrusion height and the equidistant fluctuation angle at the intersection of the spline lines were measured. The variance of protrusion height can describe the deviation from the height of the base plane, and the equidistant fluctuation angle on the base surface can describe the size of the slope and the height of the prominence. The combination of the two indexes can describe joint roughness, and the specific steps are as follows.

(1) A 3D REVscan laser scanner was used to scan fractured joint surfaces, as shown in Figure 3(a). The scanning precision of the scanner was up to 0.05 mm; the scanning speed was 18000 per second, which is approximately 40000 points per second; the scanning line width was 300 mm/beam (cross beam), and the resolution was 0.1 mm. The accuracy of the scanner could meet the calculation requirements of the joint roughness. Point cloud files were obtained after scanning, as shown in Figures 3(b) and 3(c)

(2) Point cloud files generated by scanning were introduced into the Geomagic software, which was also used to process the interval spline of the longitudinal and transverse directions of the joint surface. The spline interval was 0.5 mm (Figures 4(a) and 4(b)), and the grid with a border length of 0.5 mm × 0.5 mm was formed. An X–Y surface was set as the datum, and the 3D coordinates (X, Y, and Z) of each point of the grid were exported

(3) For the X–Y datum, the height of each point on the spline lines was obtained, as shown in Figure 4(c).

The mean height $\bar{Z}$ for the spline line was calculated as follows:

$$\bar{Z} = \frac{\sum_{i=1}^{n} Z_i}{n}, \tag{1}$$

where n is the number of points for the splines. The mean variance s of protrusion height of the spline was further obtained as follows:

$$s = \frac{1}{n}\sum_{i=1}^{n}\left(Z_i - \bar{Z}\right)^2. \tag{2}$$

The mean variance S of protrusion height of the joint surface is calculated as follows:

$$S = \bar{s}. \tag{3}$$

On the basis of the seepage direction, the fluctuation angle θ_i of the intersection points on the spline line was calculated as follows (Figure 4(c)):

$$\theta_i = \arctan\left(\frac{Z_i\text{-}Z_{i\text{-}1}}{X_i\text{-}X_{i\text{-}1}}\right). \tag{4}$$

The mean equidistant fluctuation angle $\overline{\theta}$ of the spline line was specified as

$$\overline{\theta} = \frac{\sum_{i=1}^{n}\theta_i}{n}. \tag{5}$$

The mean equidistant fluctuation angle Λ of joint surface was obtained as follows:

$$\Lambda = \overline{\overline{\theta}}. \tag{6}$$

The samples of three fractured rocks were numbered according to the order of fluctuation angle from large to small. Table 1 shows the test results.

(a) Intact CS sample (b) CS sample after splitting

(c) Intact FS sample (d) FS sample after splitting

(e) Intact MS sample (f) MS sample after splitting (g) Joint surface of three lithological samples

FIGURE 2: Joint surface of different lithological samples.

3. Stress–Seepage Coupling Test

3.1. Test Instrument and Test Principle. By using the TAW-2000M rock triaxial servo instrument shown in Figure 5, confining and water pressures were applied to the single-fracture rock sample. The water flow rate was measured in real time. On the basis of the obtained experimental data, the permeability coefficient of the sample under different working conditions was calculated.

Water pressure was applied using the pressure difference between the inlet hole of the lower end and upper outlet hole. The water pressure of the upper outlet was atmospheric pressure and was set to 0. The water pressure set in the test was the pressure difference at both ends of the sample, as shown as follows:

$$\Delta p = p_i - p_u, \tag{7}$$

where Δp is the set water pressure in the test, p_i is the water pressure of the lower inlet hole, and p_u is the water pressure of the upper outlet hole; σ_W is the set confining pressure. The test instrument and test principle are shown in Figure 6.

3.2. Test Conditions and Steps. This study mainly investigated the variation law of permeability coefficient for single-fracture rock mass affected by water pressure, confining pressure, and joint roughness. Therefore, the test condition was simplified, and the samples were only subjected to water and confining pressures without axial load. On the basis of existing research results, when the normal stress is greater than 20 MPa, the seepage flow under normal stress obviously deviates from the cubic theorem [23]. Thus, the confining pressure during the test was set to 2, 4, 6, 10, and 15 MPa, and water pressure was set to 0.5, 1.0, 1.5, 3.0, 5.0, 7.0, and 9.0 MPa (Table 2).

The assembly and sealing of the single-fracture rock sample are shown in Figure 7. The test procedure was designed as follows.

(1) The semicylindrical samples cloven from the standard cylinders were dried, vacuumed for 3.5 h, and saturated with distilled water for 48 h to ensure a single phase flow in the test samples

(2) The sample with dry surfaces was positioned between the upper and lower test bases. Silicone glue was used on both sides of the fractures. The sample was wrapped in heat-shrinkable tubes

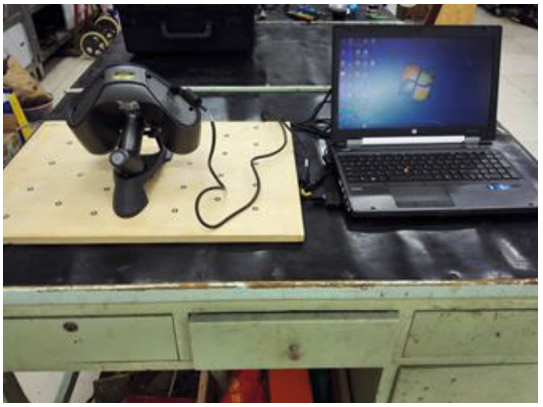

(a) 3D laser scanner

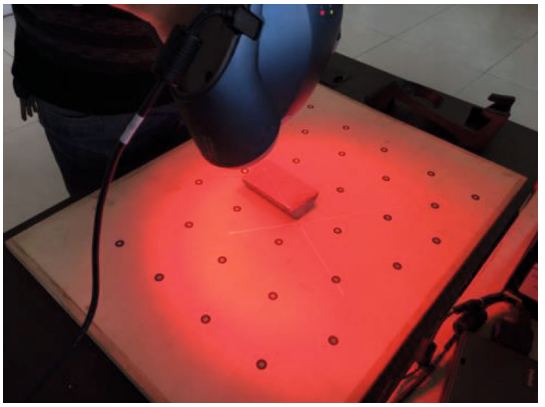

(b) Scanning sample joint surface

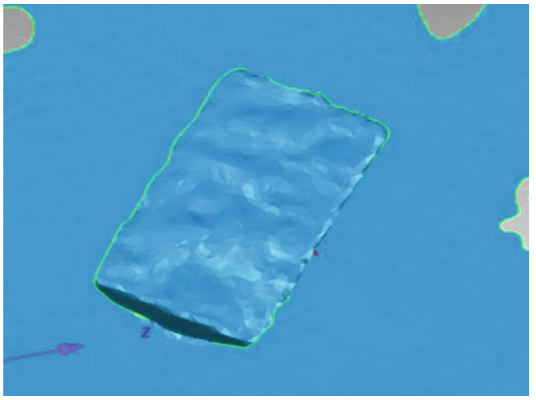

(c) Point cloud files obtained after scanning

Figure 3: 3D scanning of joint surface.

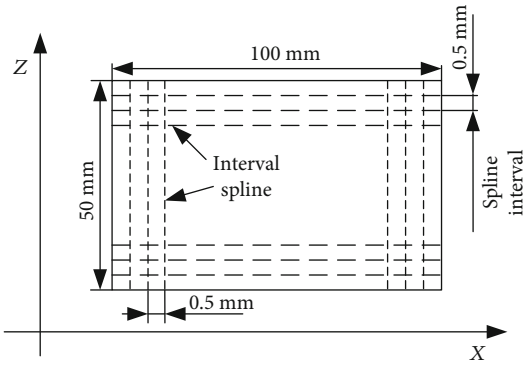

(a) Spline spacer

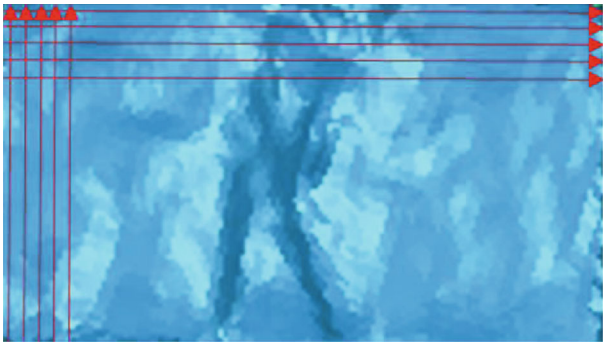

(b) Geomagic partition isometric splines

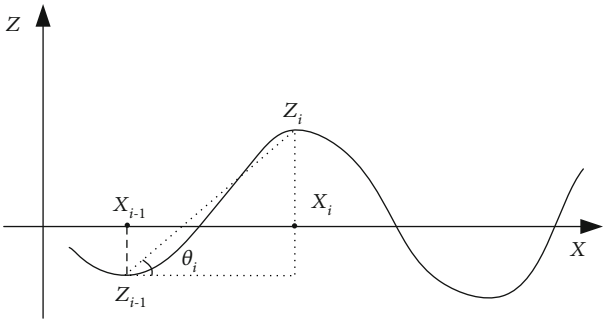

(c) Calculation of protrusion height and fluctuation angle

Figure 4: Spline interval and calculation of Geomagic.

Table 1: Roughness index measurement results of the joint surface.

	Sample number	Mean variance of protrusion height	Mean equidistant fluctuation angle (°)
CS	CS-1	5.4896	7.8956
	CS-2	4.0929	7.4568
	CS-3	2.4483	6.1982
	CS-4	1.8167	5.593
	CS-5	1.0138	5.0429
	CS-6	0.5729	4.7844
FS	FS-1	9.6780	10.10
	FS-2	9.5402	8.17
	FS-3	7.0203	8.16
	FS-4	6.5496	7.86
	FS-5	5.6889	5.24
	FS-6	4.3265	3.43
MS	MS-1	14.1871	29.30
	MS-2	14.2546	34.56
	MS-3	13.2056	23.01
	MS-4	12.4556	22.01
	MS-5	10.8990	18.06
	MS-6	9.7888	14.56

(3) The extensometers and hoop devices were installed to the sample that had been handled after 24 h. The extensometers included axial and radial extensometers, and the hoop devices included a hoop and a rubber ring

(4) The assembled samples were placed on the cylinder connection base in the test machine and were connected to the axial extensometer, radial extensometer, and inlet and outlet pipes. A pretest with water was ensured that the system was sealed well

(5) After sample installation and the pretest, the triaxial pressure chamber was lowered, and the oil pressure and hydraulic systems were connected to the sample base. The oil tank was filled to the desired level

(6) In the test, confining pressure was initially applied, and water pressure was applied. After the water pressure became stable, the flow in this time period was measured and recorded. The record was completed, the water pressure was increased gradually, and the flow rate under each level of water pressure was measured and recorded. The confining pressure level was increased, and the water pressure was loaded repeatedly

(7) During the loading process, the original data obtained were the total amount (Q) of time (t) for the duration of a certain working condition. The derivative of the total flow to the time was the velocity (q) of the flow. When the permeability coefficient reached the set value, flow was linear to time. To ensure measurement accuracy, the linear steady growth continued for 30 min, and the slope of the straight line was fitted. Taking CS-3 as an example, the confining pressure of 2 MPa was kept constant, and the water pressure was set from 0.5 MPa to 1.0-1.5 MPa. The relationship between flow and time was recorded, and the slope of a straight line was q, as shown in Figure 8

(8) Under the working condition of constant pressure and stable water pressure, the seepage flow in the sample is in accordance with Darcy's law. By bringing the flow rate q and water pressure Δp into Eq. (8), the permeability coefficient of the sample was calculated as follows [24]:

$$k = \frac{qL\gamma_w}{\Delta pA} \mathrm{X}10^{-3}, \tag{8}$$

where k is the coefficient of permeability (cm/s), q is the seepage quantity of rock samples (mL/s), L is the sample length, γ_w is the unit weight of water (9.81 kN/m^3), A is the cross-sectional area of the sample (cm^2), and Δp is the fracture water pressure difference between the two ends of the sample (MPa).

(9) When the confining pressure is constant, the water pressure is reduced to the initial value, and then, repeated loading is added to the water pressure, and the same experimental results can be obtained. The test was completed, the sample was removed, and the experimental pressure head was cleaned after the completion of the experiment. The inlet and outlet channels were guaranteed to be smooth

3.3. Realization and Determination of Seepage Flow along Rock Fracture

3.3.1. Realization of Seepage Flow along Rock Fracture. Many factors influence the seepage test of fracture rock. Controlling the test process and realizing flow seepage along rock fracture are difficult. In this study, the installation and test methods were improved by analyzing the test process and phenomena and summing up the failure experience.

(1) Under the action of water pressure, the pressurized water flowing along the fracture could easily penetrate into the gap between the sample and the thermoplastic tube, which would have a great influence on the results of the seepage test, as shown in Figure 9

The pressurized water was also permeable at the joints between the sample and the permeable gasket and upper and lower pressure heads, as shown in Figure 10.

On the basis of the above analysis, the silicone rubber with a 5 mm width and 3 mm thickness was used to seal both sides of lateral fracture and joints, and the outer layer was wrapped with adhesive tape. The silicone rubber has good sealing performance, which can prevent the pressurized water from entering the sample lateral from the lateral fracture and joints. The same arc steel gasket was added to the crack side, as shown in Figures 7(a)–7(e).

(a) Pressure chamber (b) Pressurization system (c) Computer control system

Figure 5: TAW-2000M rock triaxial servo instrument.

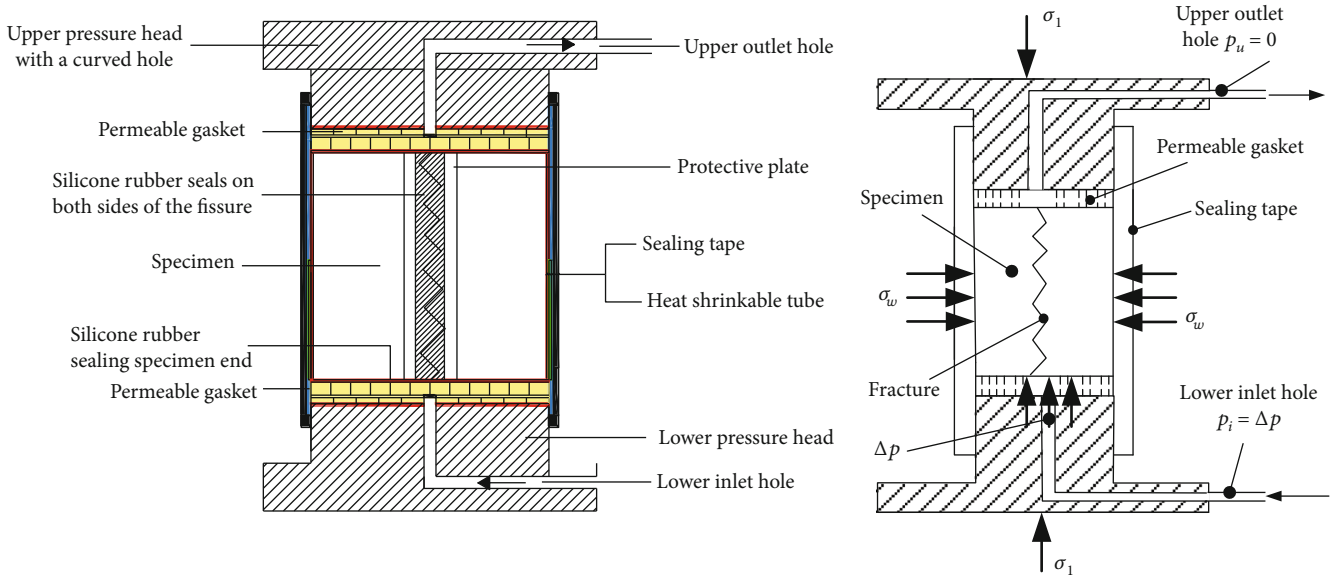

(a) Sample assembly diagram for seepage test (b) Principle diagram for seepage test

Figure 6: Sample assembly and principle diagram for seepage test.

(2) Under the condition of high confining pressure and low water pressure, the heat shrinkable pipe was easily pressed through the oil pressure of high confining pressure at the depression of sample. This condition formed the confining pressure and water pressure penetration, which led to the failure of the test, as shown in Figure 11. Therefore, in the sample selection, strictly selecting the complete samples after splitting was necessary

(3) The contact part of thermoplastic pipe and the upper and lower pressure heads was the weak point. When the difference between the confining and water pressures was large, the seal was not strict, which would form the through and lead to the failure of the test. Moreover, the smoothness of the joint should be ensured when the sample was installed

3.3.2. Determination of Seepage Flow along Rock Fracture. Seepage test was performed in the oil tank. Whether the water passed only through the fracture and whether the unidirectional flow was achieved were keys for data adoption.

Samples were dried before the sample was installed. After the seepage test was completed, if the sample surface was dry and the joint surface had clear watermarks, then the unidirectional flow of the pressurized water along the fracture was achieved, as shown in Figure 12.

If a water trace was evident on the outer surface of the sample, then water flow was observed into the gap between the sample and the thermoplastic pipe, and the test would fail. If oil trace was found on the surface of the sample or water and confining pressure was the same and could not be adjusted in the test process, then the heat shrinkable tube was pressed through, and the test was determined to fail (Figure 13).

4. Analysis of Stress–Seepage Coupling Mechanism

4.1. Effects of Confining and Water Pressures on Permeability Coefficient. The loading path was constant confining pressure, and the water pressure was loaded gradually. The seepage tests of CS, FS, and MS were performed, and the

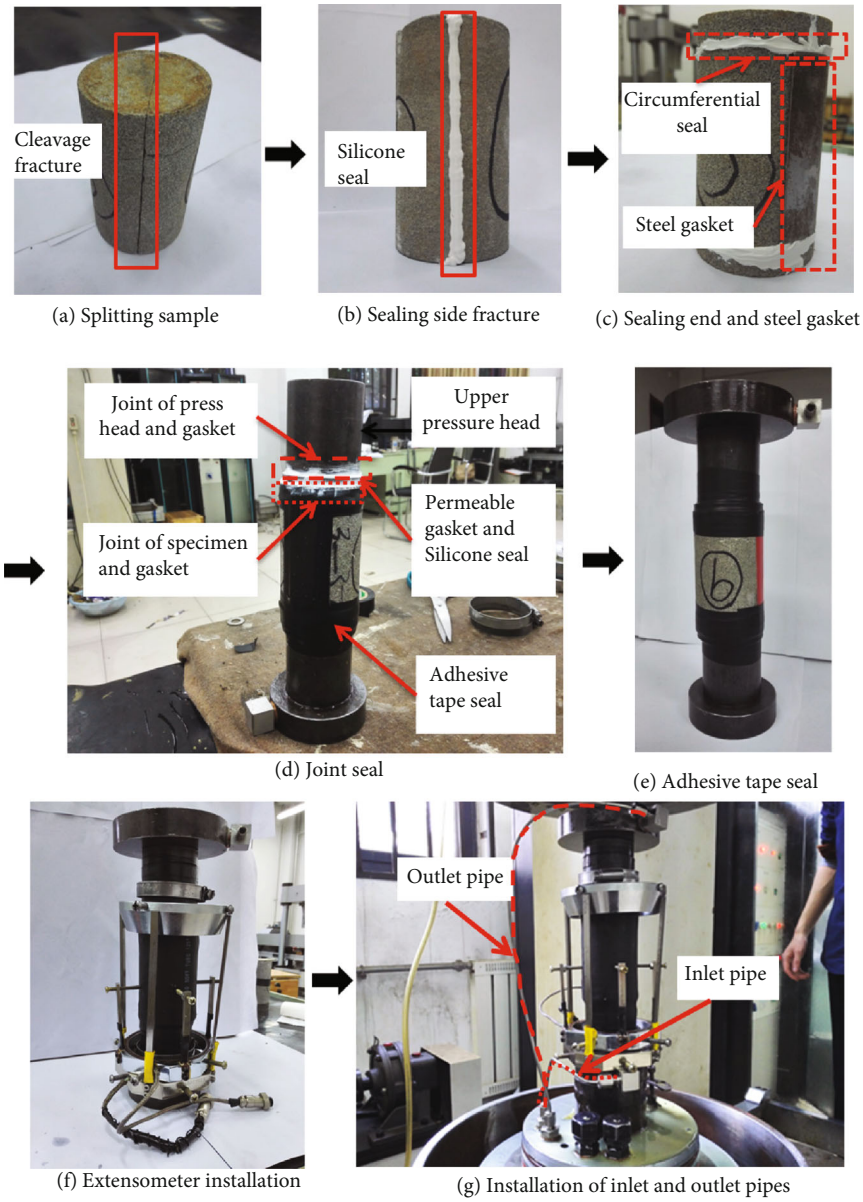

Figure 7: Sample mounting process: (a) splitting sample; (b) sealing side fracture; (c) sealing end and steel gasket; (d) joint seal; (e) adhesive tape seal; (f) extensometer installation; (g) installation of inlet and outlet pipes.

Table 2: Seepage test load.

Sample number	Confining pressure (MPa)	Water pressure (MPa)	Duration (min)
CS-1–6 FS-1–6 MS-1–6	2, 4, 6, 10, 15	0.5, 1.0, 1.5, 3.0, 5.0, 7.0, 9.0	30

permeability coefficient under different working conditions was obtained. Some data of the CS-1 sample are shown in Table 3.

Under the condition of constant confining pressure, the influence of water pressure on permeability coefficient is shown in Figures 14–16, and three samples were taken for each lithological sample.

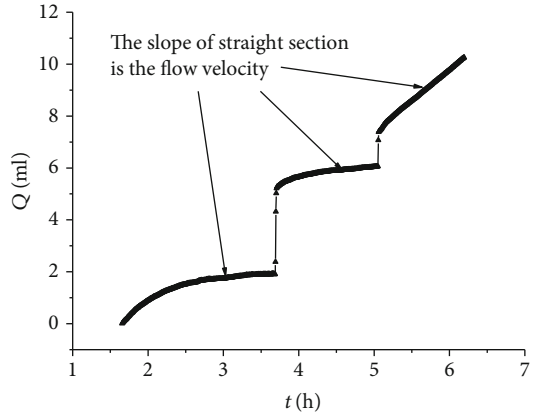

Figure 8: Relationship between Q and $t(\sigma_W = 3\text{MPa})$.

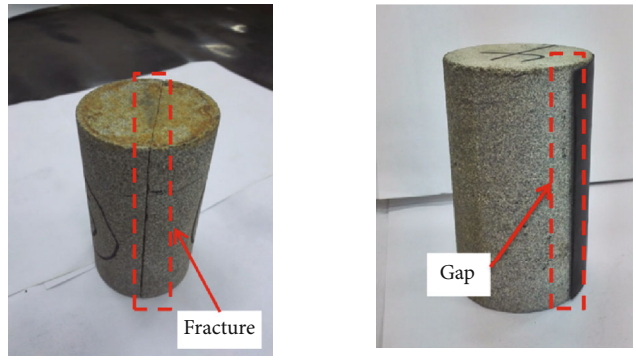

(a) Lateral fracture (b) Gap between sample and thermoplastic tube

Figure 9: Fracture and the gap between sample and thermoplastic tube.

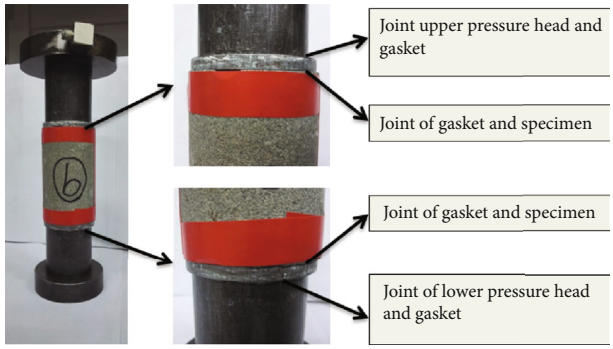

Figure 10: Gap between the sample and permeable gasket and upper and lower pressure heads.

The analysis of Figures 14–16 shows that under constant confining pressure, permeability coefficient and water pressure have a linear growth relationship, which can be expressed as

$$k = A\Delta p, \tag{9}$$

where A is the linear slope and is related to joint roughness.

The analysis of Darcy's law indicates that if the seepage is laminar flow and fracture aperture is constant, then the permeability coefficient does not change with water pressure; under the same test condition, the test result in this study is consistent with Darcy's law. With the change of test condition, the test result in this study is inconsistent with Darcy's law. That is, the permeability coefficient is influenced not only by the variation of water pressure but also by the change of confining pressure. The reasons are as follows.

(1) When the water pressure inside the fracture increases and hydraulic splitting effect is produced, the two sides of rock mass produce a small normal deformation, the contact area in the fracture decreases, and fracture aperture and permeability coefficient increase

(2) When the water pressure inside the fracture is smaller than 10 MPa, the normal deformation of rock mass on both sides of the fracture is relatively large, and the influence on permeability coefficient is significant. When the confining pressure is greater than 10 MPa, the water pressure inside the fracture is relatively small compared with the normal stress, and the fracture aperture is only a residual aperture. The existence of high confining pressure makes the normal deformation under water pressure limited, and the fracture aperture variation is small. When the confining pressure is relatively large, the influence of water pressure on permeability coefficient is also small

Figure 11: Thermoplastic pipe breakdown for high confining pressure at sample depression.

The relationship between permeability coefficient and confining pressure of the three lithological samples of CS, FS, and MS is shown in Figures 17–19, respectively.

As shown in Figures 17–19, the permeability coefficient of fractured rock mass decreases with the increase of confining pressure. However, as the confining pressure increases, the attenuation rate of the permeability coefficient is different. When the confining pressure is less than 10 MPa, the permeability coefficient decreases sharply with the increase of confining pressure. When the confining pressure is greater than 10 MPa, as the confining pressure increases, the decrease of the permeability coefficient becomes slow and finally tends to become a constant value.

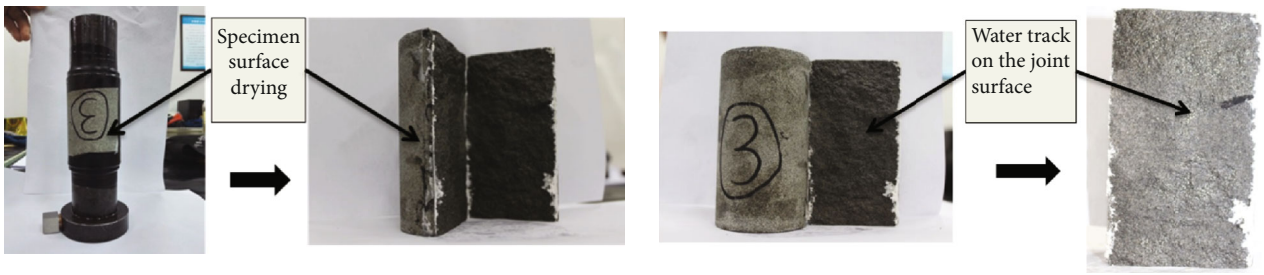

(a) Sample surface drying for achieving single-fracture seepage (b) Water track on the joint surface for achieving single-fracture seepage

Figure 12: Sample characteristics for achieving single-fracture seepage.

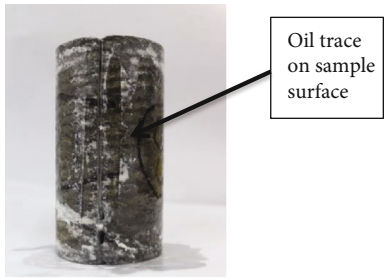

Figure 13: Oil-stained sample.

Under the condition of constant water pressure, the relationship between permeability coefficient and confining pressure is fitted, and the permeability coefficient is negatively correlated with the confining pressure. Taking CS-1 as an example, when the water pressure is 0.5, 1.0, and 1.5 MPa, the relationship between confining pressure and permeability coefficient is shown in Figure 20.

The relationship between permeability coefficient and confining pressure can be expressed by a negative exponential function, that is,

$$k = a_1 \exp(-a_2 \sigma_n), \tag{10}$$

where a_1 and a_2 are the fitting parameters obtained by the test results and are related to the roughness of the joint surface.

4.2. Effects of Different Lithological Joints on Permeability Coefficient. Here, CS-1, FS-1, and MS-1, with confining pressure of 2 MPa and water pressure 0.5 MPa, are taken as examples, as shown in Figure 21. Given the different lithologies, the joint roughness obtained after splitting is different, and the permeability coefficient is relatively different under the same working condition. The permeability coefficient of CS is larger than that of FS and that FS is larger than that of MS.

4.3. Derivation of Permeability Coefficient Formula considering Joint Roughness. The test results indicate that the functional relationship between permeability coefficient and hydraulic or confining pressure can be obtained by Eqs. (9) and (10), as shown as follows:

$$k = A a_1 \exp(-a_2 \sigma_n) \Delta p. \tag{11}$$

Table 3: Test value of permeability coefficient of CS-1 sample (unit: $\times 10^{-8}$ cm/s).

Water pressure (MPa)	Confining pressure (MPa)				
	2	4	6	10	15
0.5	2.6403	1.7526	1.2497	0.5867	0.1593
1.0	9.1492	2.6971	1.6380	0.6620	0.1931
1.5	14.8280	3.8188	1.9794	0.6977	0.2565
2		4.6878	2.1414	0.7265	0.3190
2.5		5.7841	2.4469	0.7822	0.3785
3		7.2458	2.7069	0.8305	0.4049
5			4.2924	0.9372	0.4394
7				1.4529	0.5409
9					0.8308

Coefficients A, a_1, and a_2 are parameters related to joint roughness. Under the same condition, taking CS, with confining pressure of 6 MPa and water pressure of 1.5 MPa, as an example, the relationship between coefficients A, a_1, and a_2 and the mean variance of protrusion height S or the mean equidistant fluctuation angle Λ were fitted, as shown in Figure 22. The relationship between A, a_1, and a_2 and S and Λ has an approximately linear correlation.

Thus, A, a_1, and a_2 can be expressed as

$$\begin{aligned} A &= (d1S + d_2)(d3\Lambda + d4), \\ a1 &= \left(d_1{}'S + d_2{}'\right)\left(d_3{}'\Lambda + d4'\right), \\ a2 &= \left(d_1{}''S + d_2{}''\right)\left(d_3{}''\Lambda + d4''\right), \end{aligned} \tag{12}$$

where $d_1, d_2, d_3, d_4, d_1{}', d_2{}', d_3{}', d_4{}', d_1{}'', d_2{}'', d_3{}'', d_4{}''$, and $d_4{}''$ are the fitting constants. By substituting Eq. (12) into Eq. (11), k can be expressed as

$$\begin{aligned} k = (d1S + d_2)(d3\Lambda + d4)\left(d_1{}'S + d_2{}'\right)\left(d_3{}'\Lambda + d4'\right) \\ \exp\left[-\left(d_1{}''S + d_2{}''\right)\left(d_3{}''\Lambda + d4''\right)\sigma_n\right]\Delta p. \end{aligned} \tag{13}$$

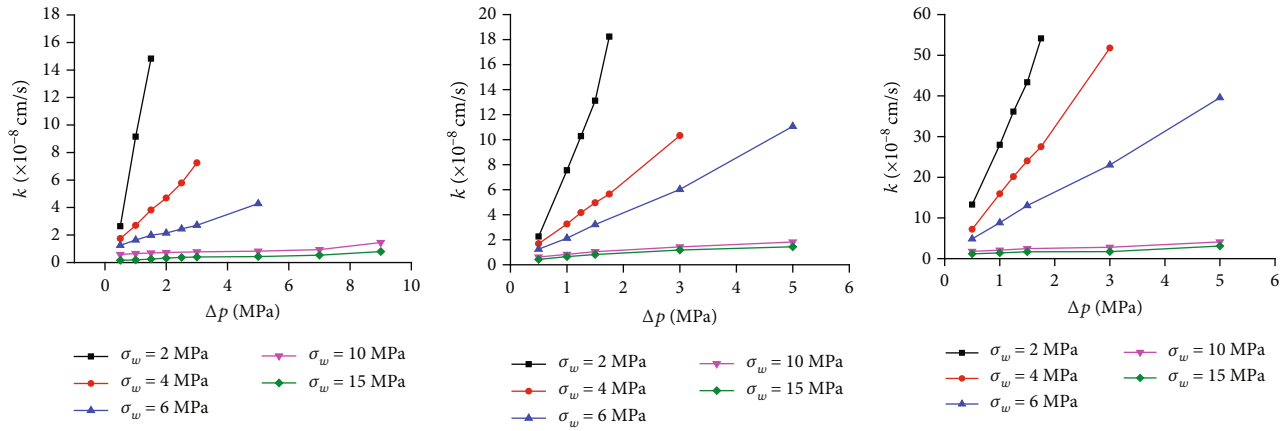

(a) CS-1 (b) CS-2 (c) CS-3

Figure 14: Relationship between permeability coefficient and water pressure for CS.

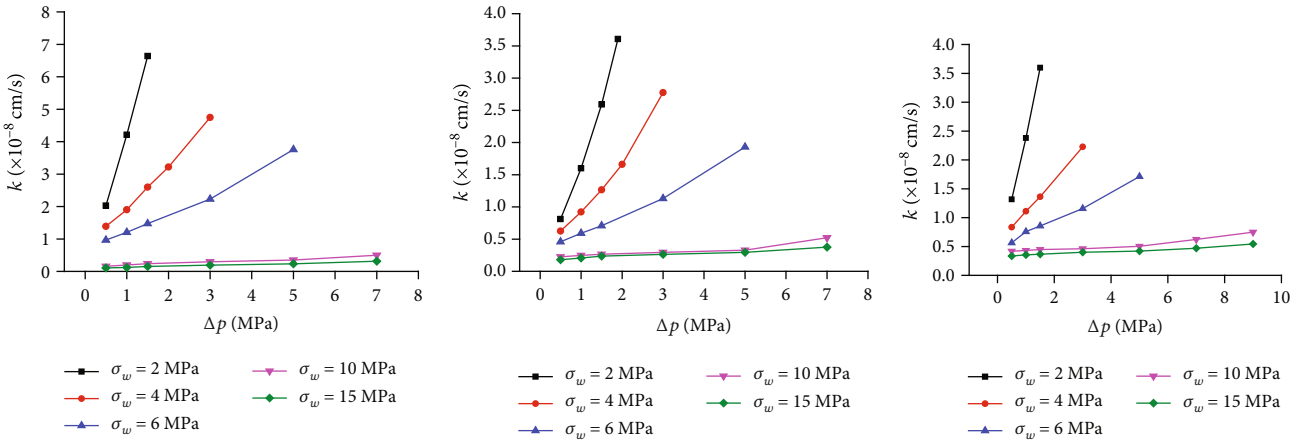

(a) FS-1 (b) FS-2 (c) FS-3

Figure 15: Relationship between permeability coefficient and water pressure for FS.

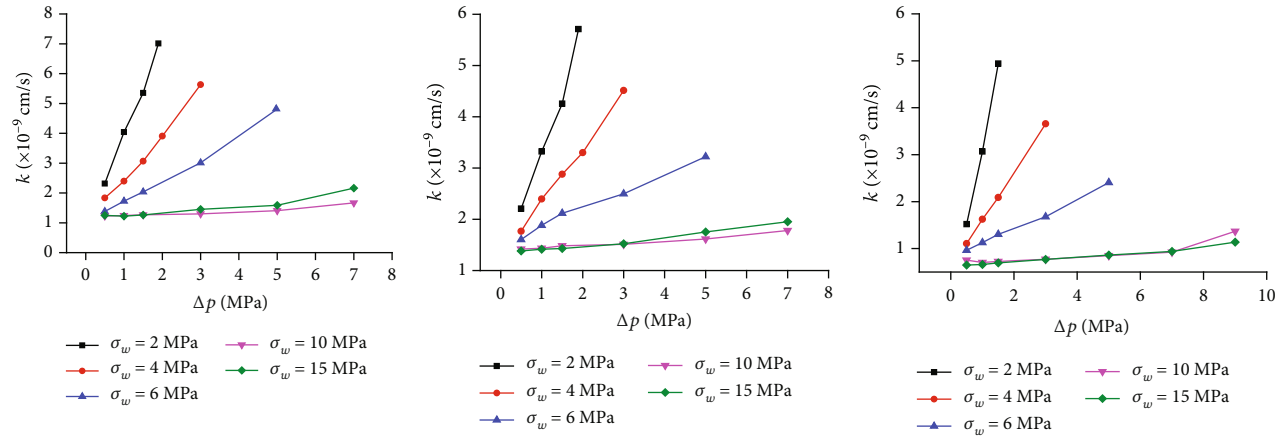

(a) MS-1 (b) MS-2 (c) MS-3

Figure 16: Relationship between permeability coefficient and water pressure for MS.

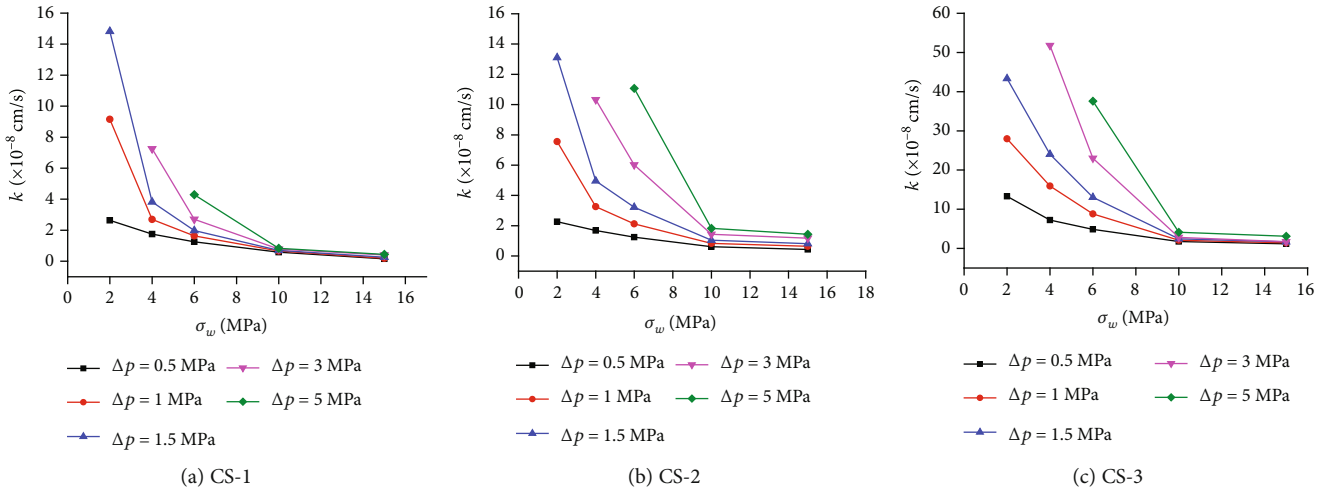

Figure 17: Relationship between permeability coefficient and confining pressure for CS.

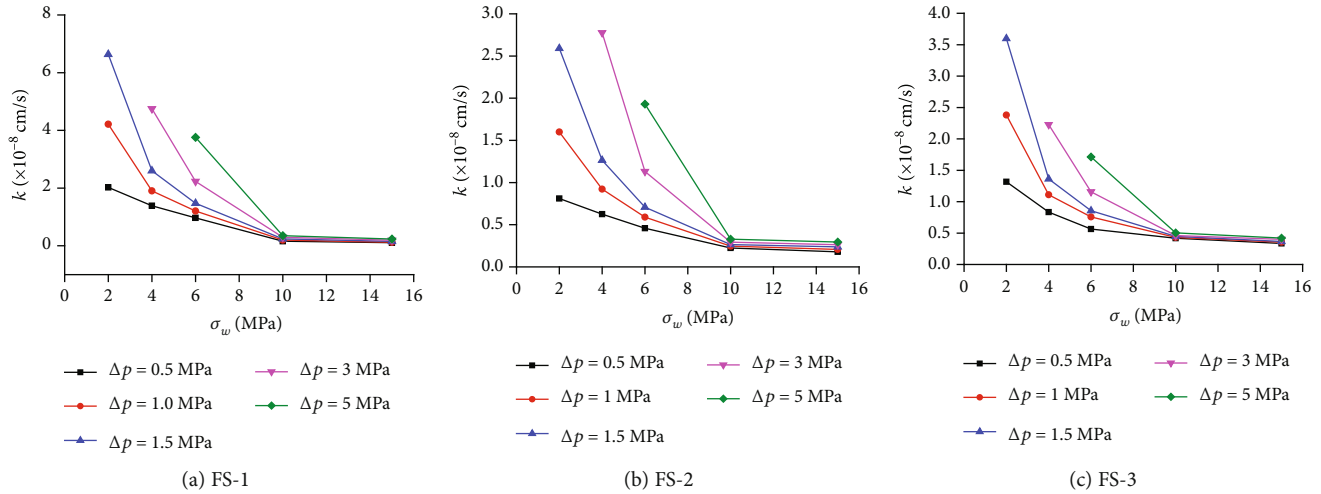

Figure 18: Relationship between permeability coefficient and confining pressure for FS.

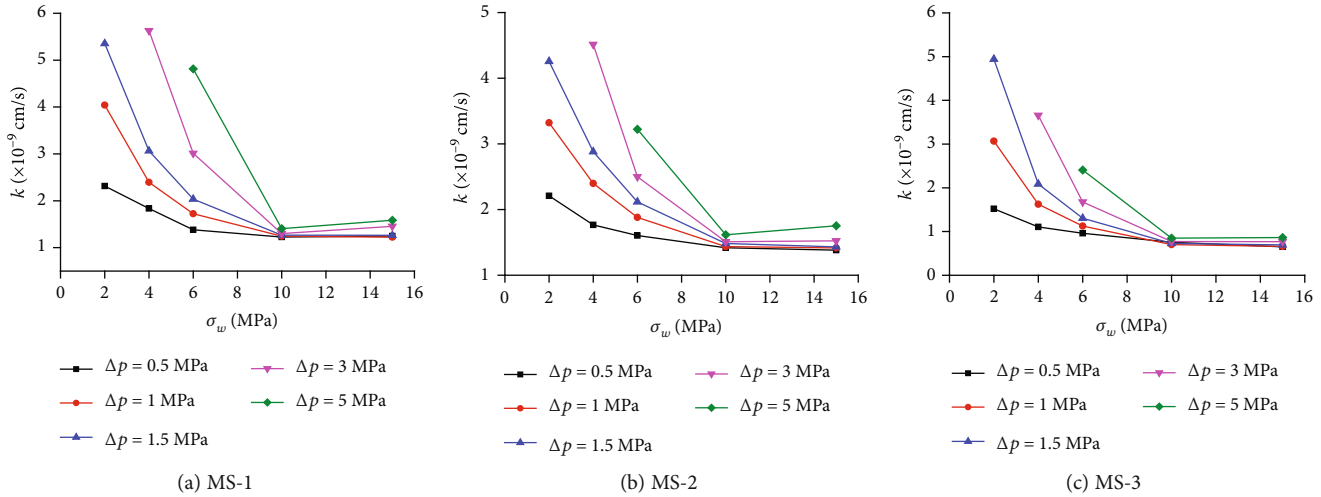

Figure 19: Relationship between permeability coefficient and confining pressure for MS.

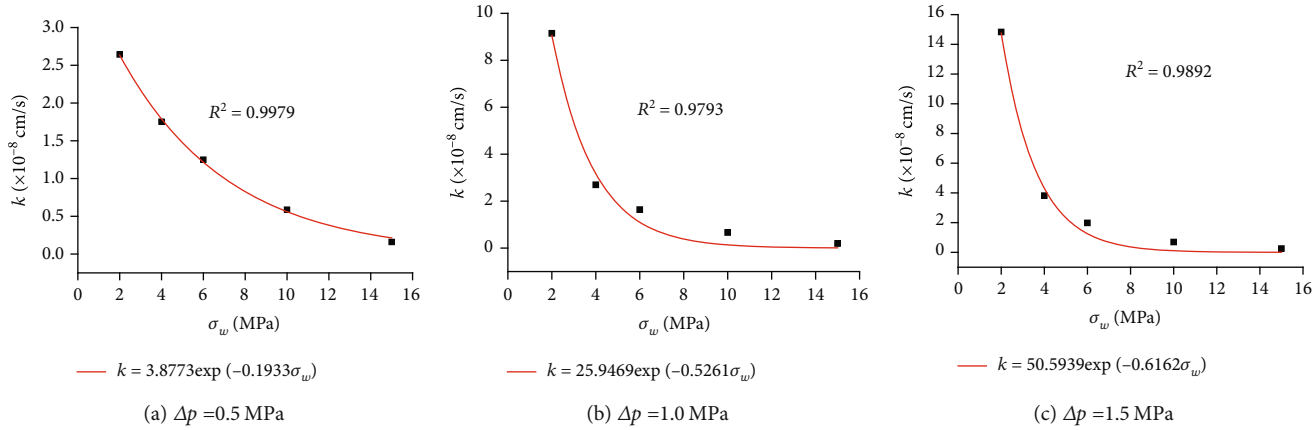

(a) Δp =0.5 MPa (b) Δp =1.0 MPa (c) Δp =1.5 MPa

Figure 20: Relationship between permeability coefficient and confining stress under constant water pressure.

k is further expressed as

$$k = \left(c_1 S^2 + c_2 S + c_3\right)\left(c_1{}' \Lambda^2 + c_2{}' \Lambda + c_3{}'\right) \exp \left[-\left(d_1{}'' S + d_2{}''\right)\left(d_3{}'' \Lambda + d4''\right)\sigma_n\right] \Delta p, \quad (14)$$

where c_1, c_2, c_3, $c_1{}'$, $c_2{}'$, $c_3{}'$, and $c_3{}'$ are fitting constants. The k function in Eq.(14) contains confining pressure σ_w, water pressure Δp, the mean variance of protrusion height S, and the mean equidistant fluctuation angle Λ, which effectively describe the influence of geometric shape parameters of the fracture surface on the permeability coefficient.

According to the test results (CS sample, confining pressure 6 MPa, water pressure 1.5 MPa), the relationship between k and S or Λ was fitted, as shown in Figure 23.

The function relationships k and S or Λ can be expressed as exponential relationships:

$$k = \left(c_1 S^2 + c_2 S + c_3\right) \exp\left(-c_4 S + c_5\right), \quad k = \left(c_1{}' \Lambda^2 + c_2{}' \Lambda + c_3{}'\right) \exp\left(-c_4{}' \Lambda + c_5{}'\right), \quad (15)$$

where c_4, c_5, $c_4{}'$, and $c_5{}'$ are fitting constants. It can be seen that in Eq. (15), when any value of S and Λ is constant, the relationship between k and S or Λ can be expressed as an exponential function, which verifies the accuracy of Eq. (14). The variance of protrusion height S is used to describe the deviation of joint surface protrusion, and the equidistant fluctuation angle Λ is used to describe the height of joint surface protrusion. The larger the value of S and Λ is, the smaller the value of k is, which indicates that the more dispersed and high the protrusion on joint surface is, the greater the obstruction of joint surface to water flow is.

5. Conclusion

The seepage characteristics of fractured rock mass are closely related to joint roughness, surrounding rock pressure, and water pressure. In this study, the law of seepage in fractured rock mass is explored through the effective measurement of joint roughness and a large number of seepage tests.

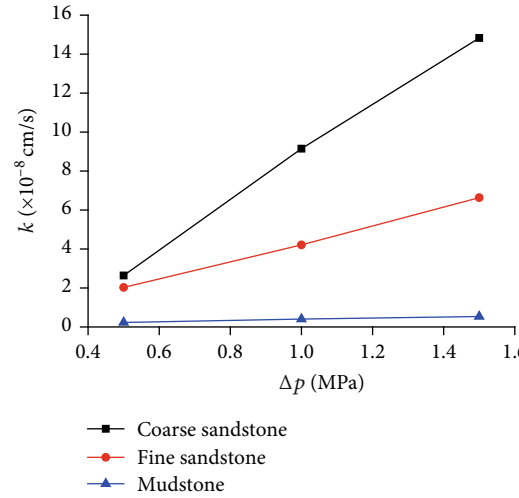

Figure 21: Comparison of three permeability coefficients (σ_w =2 MPa, Δp=0.8 MPa).

(1) When the confining pressure was constant and water pressure was graded loading, the permeability coefficient and water pressure had a positive linear relationship, whereas the permeability coefficient and confining pressure had a negative exponential relationship. With the increase of confining pressure, the influence of water pressure on permeability coefficient gradually decreased, the confining pressure increased to a certain value, the width of the fracture was only the width of the residual gap, and the permeability coefficient tended to be stable

(2) On the basis of the relationship of permeability coefficient and water pressure or confining pressure, the relationship between expression coefficient and the mean variance of protrusion height or equidistant fluctuation angle was fitted, and the calculation formula including joint roughness, water pressure, and

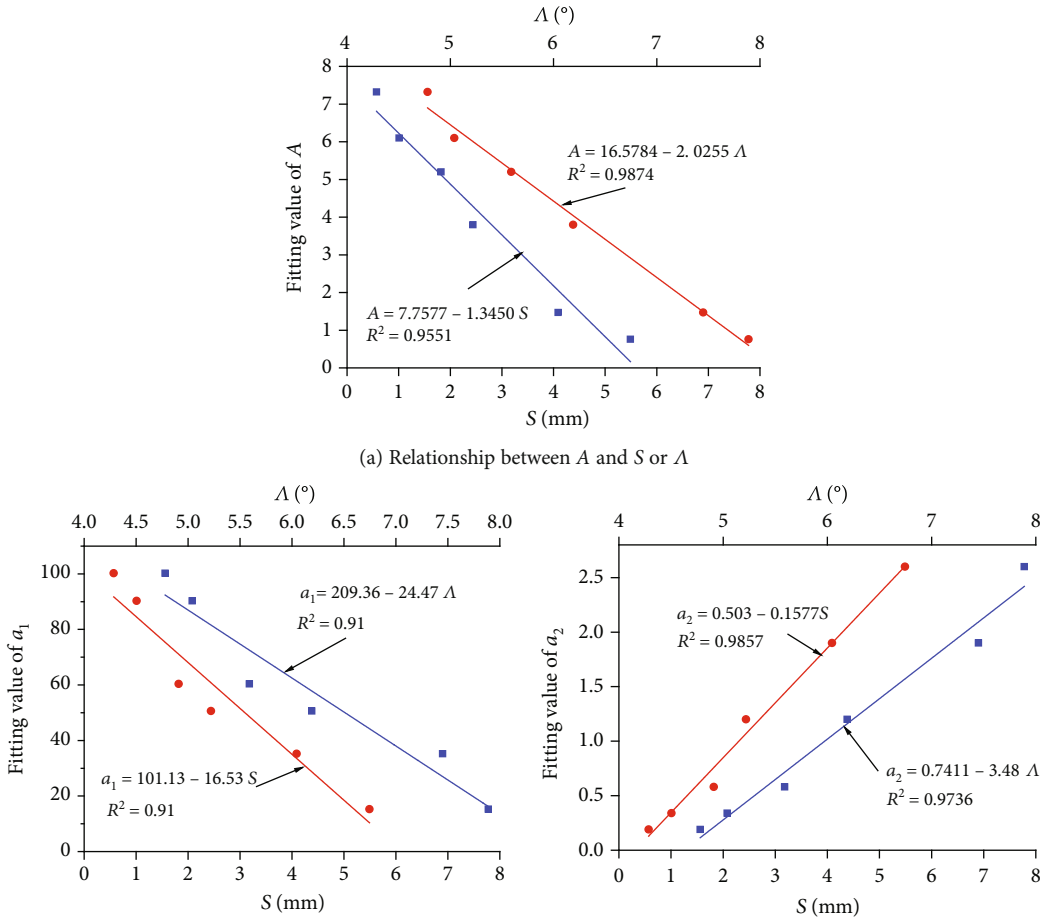

(a) Relationship between A and S or Λ

(b) Relationship between a_1 and S or Λ

(c) Relationship between a_2 and S or Λ

Figure 22: Relationship between A, a_1, and a_2 and S and Λ.

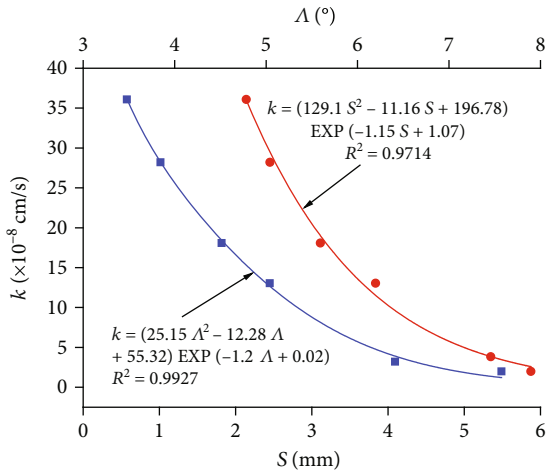

Figure 23: Relationship between k and S or Λ.

confining pressure is derived. In the process of rocked mass fracture seepage, the protrusion on joint surface hinders the water flow. While the protrusion height is higher and more dispersed, the obstruction of joint surface to water flow is greater, and the permeability coefficient of fractured rock mass is smaller

Data Availability

The data used to support the findings of this study are available from the corresponding author upon request.

Conflicts of Interest

The authors declare that they have no conflicts of interest.

Acknowledgments

This project is supported by the National Natural Science Foundation of China (Grant No. 51774196), the China Postdoctoral Science Foundation (No. 2016M592221), the Research Fund of Liaocheng University (No. 258481, 318051848), and the Natural Science Foundation of Shandong Province (No. ZR2017MEE069).

References

[1] D. T. Snow, "Rock fracture spacings, openings and porosities. Journal of Soil Mechanics and Foundations Division," *ASCE*, vol. 94, no. 1, pp. 73–92, 1968.

[2] Louisc, "*Rock hydraulics. Rock mechanics*," Springer Wien, New York, 1974.

[3] D. T. Snow, *A Parallel Plate Model of Fractured Permeable Media*, University of California, Berkeley, Berkeley, 1965.

[4] G. Wang, N. Huang, Y. J. Jiang, B. Li, W. Xuezhen, and X. Zhang, "Seepage calculation model for rough joint surface considering fractal characteristics," *Chinese Journal of Rock Mechanics and Engineering*, vol. 33, Supplement 2, pp. 3397–3405, 2014.

[5] D. Vogler, R. R. Settgast, C. Annavarapu, C. Madonna, P. Bayer, and F. Amann, "Experiments and simulations of fully hydro-mechanically coupled response of rough fractures exposed to high-pressure fluid injection," *Journal of Geophysical Research: Solid Earth*, vol. 123, no. 2, pp. 1186–1200, 2018.

[6] J. Zhao, L. Yin, and W. Guo, "Stress–seepage coupling of cataclastic rock masses based on digital image technologies," *Rock Mechanics and Rock Engineering*, vol. 51, no. 8, pp. 2355–2372, 2018.

[7] C. Wang, Y. Jiang, R. Liu, C. Wang, Z. Zhang, and S. Sugimoto, "Experimental study of the nonlinear flow characteristics of fluid in 3D rough-walled fractures during shear process," *Rock Mechanics and Rock Engineering*, vol. 53, no. 6, pp. 2581–2604, 2020.

[8] C. Wang, Y. Jiang, H. Luan, and S. Sugimoto, "Effect of shearing on hydraulic properties of rough-walled fractures under different boundary conditions," *Energy Science & Engineering*, vol. 8, no. 3, pp. 865–879, 2020.

[9] B. S. A. Tatone and G. Grasselli, "An investigation of discontinuity roughness scale dependency using high-resolution surface measurements," *Rock Mechanics and Rock Engineering*, vol. 46, no. 4, pp. 657–681, 2013.

[10] L. Zou, L. Jing, and V. Cvetkovic, "Roughness decomposition and nonlinear fluid flow in a single rock fracture," *International Journal of Rock Mechanics and Mining Sciences*, vol. 75, pp. 102–118, 2015.

[11] Y. J. Jiang, B. Li, G. Wang, and S. C. Li, "New advances in experimental study on seepage characteristics of rock fractures," *Chinese Journal of Rock Mechanics and Engineering*, vol. 27, no. 12, pp. 2377–2386, 2008.

[12] G. Wang, X. P. Zhang, Y. J. Jiang, B. Li, X. Z. Wu, and N. Huang, "Meso-mechanism research on shear failure of rock joint based on particle discrete element method," *Journal of Central South University (Science and Technology)*, vol. 46, no. 4, pp. 1442–1453, 2015.

[13] B. Zhang and Z. Meng, "Experimental study on floor failure of coal mining above confined water," *Arabian Journal of Geosciences*, vol. 12, no. 4, 2019.

[14] X. Z. Lyu, Z. Zhao, X. Wang, and W. Wang, "Study on the permeability of weakly cemented sandstones," *Geofluids*, vol. 2019, Article ID 8310128, 14 pages, 2019.

[15] J. Liu, J. L. Li, J. J. Qu, and Y. D. Zhang, "Experimental study on seepage in cranny of sandstone due to axial compression and artificial fracture," *Journal of Hydrographic Engineering*, vol. 41, no. 2, pp. 1461–1468, 2010.

[16] H. D. Yu, F. F. Cheng, J. P. Yang, J. J. Cong, and K. K. Guo, "Research on permeability of fractured rock," *Chinese Journal of Rock Mechanics and Engineering*, vol. 31, Supplement 1, pp. 2788–2795, 2012.

[17] M. Souley, P. Lopez, M. Boulon, and A. Thoraval, "Experimental hydromechanical characterization and numerical modelling of a fractured and porous sandstone," *Rock Mechanics and Rock Engineering*, vol. 48, no. 3, pp. 1143–1161, 2015.

[18] B. H. Guo and C. D. Su, "Test research on piecewise seepage characteristics of rock fracture under multistage loadings," *Chinese Journal of Rock Mechanics and Engineering*, vol. 31, Supplement 2, pp. 3787–3794, 2012.

[19] Y. Hu, Y. Y. Ye, G. T. Liu, and P. H. Li, "Experiment research on the laws of seepage in calcirudite rock within single fracture under multiaxial stresses," *Chinese Journal of Underground Spaceand Engineering*, vol. 3, no. 6, pp. 1009–1013, 2007.

[20] J. Liu, Y. U. Zhenmin, R. Wang, and L. Jianlin, "Research on seepage law of splitting sandstone with non-fillers under multiple factors," *Journal of Hydrographic Engineering*, vol. 47, no. 1, pp. 54–63, 1994.

[21] H. Yang, *Experimental Study on Permeability Coefficient in Fractured Rock Mass of Tunnel*, Shijiazhuang Tiedao University, Shijiazhuang, 2015.

[22] Z. Tian, W. Zhang, C. Dai, B. Zhang, Z. Ni, and S. Liu, "Permeability model analysis of combined rock mass with different lithology," *Arabian Journal of Geosciences*, vol. 12, no. 24, 2019.

[23] Y. T. Zhang, *Movement of Water in Fractured Rock Mass and its Interaction with Hydraulic Structures*, Tianjin University Press, Tianjin, 1992.

[24] L. H. Xu and N. Xie, "Test and theoretical research on permeability characteristics of shear fracture in rock mass," *Chinese Journal of Rock Mechanics and Engineering*, vol. 28, no. 11, pp. 2249–2257, 2009.